

Changes in Polarization Position Angle across the Eclipse in the Double Pulsar System

R. Yuen^{1,2}, R. N. Manchester¹, M. Burgay³, F. Camilo⁴, M. Kramer⁵, D. B. Melrose² and I. H. Stairs⁶

¹*CSIRO Astronomy and Space Science, Australia Telescope National Facility, P.O. Box 76, Epping, NSW 1710, Australia*

²*SIfA, School of Physics, the University of Sydney, NSW 2006, Australia*

³*INAF-Osservatorio Astronomica di Cagliari, Loc. Poggio dei Pini, Strada 54, 09012 Capoterra, Italy*

⁴*Columbia University, New York, NY 10027, USA*

⁵*Max Planck Institut für Radioastronomie, Auf dem Hügel 69, 53121 Bonn, Germany*

⁶*Department of Physics and Astronomy, University of British Columbia, Vancouver, BC V6T 1Z1, Canada*

ABSTRACT

We investigate the changes in polarization position angle in radiation from pulsar A around the eclipse in the Double Pulsar system PSR J0737-3039A/B at the 20 cm and 50 cm wavelengths using the Parkes 64-m telescope. The changes are $\sim 2\sigma$ during and shortly after the eclipse at 20 cm but less significant at 50 cm. We show that the changes in position angle during the eclipse can be modelled by differential synchrotron absorption in the eclipse regions. Position angle changes after the eclipse are interpreted as Faraday rotation in the magnetotail of pulsar B. Implied charge densities are consistent with the Goldreich-Julian density, suggesting that the particle energies in the magnetotail are mildly relativistic.

Subject headings: binaries: eclipsing — polarization — pulsars: individual (PSR J0737-3039A, PSR J0737-3039B)

1. Introduction

PSR J0737-3039A/B, also known as the Double Pulsar system, is a compact binary system consisting of two neutron stars, both radiating at radio frequencies¹. Discovered by Burgay et al. (2003) and Lyne et al. (2004) in a survey at 20 cm wavelength using a multibeam receiver on the 64-m radio telescope at Parkes in New South Wales, Australia, the two pulsars, referred to as pulsar A and pulsar B respectively, orbit each other with a period of about 2.45 hours in an almost circular trajectory with eccentricity 0.088 (Burgay et al. 2003; Kramer et al. 2006). The inclination angle between the line of sight and orbital plane normal is estimated to be 87.7° . The spin periods for pulsar A and B are $P_A = 22.7$ ms and $P_B = 2.77$ s, and their surface dipole magnetic field strengths are $B_A = 6.3 \times 10^9$ G and $B_B = 1.2 \times 10^{12}$ G. The spin-down powers for pulsar A and B are $\dot{E}_A \sim 5.9 \times 10^{33}$ erg s⁻¹ and $\dot{E}_B \sim 1.6 \times 10^{30}$ erg s⁻¹, giving $\dot{E}_A/\dot{E}_B \sim 3500$.

Because of the strong relativistic wind from pulsar A, the magnetosphere of pulsar B is truncated compared to that of an isolated pulsar. The relativistic particle flux in the wind penetrates into the light cylinder of B resulting in the formation of a bow shock that strongly perturbs the dipolar field structure by compressing B’s magnetosphere on the “daytime” side (the side facing A), and stretching it on the “nighttime” side into a magnetotail. From studies on simulating the interaction between A’s wind and B’s magnetosphere (Arons et al. 2004), the magnetotail probably reaches a distance of several semi-major axes of pulsar B’s orbit (the semi-major axis is 4.5×10^8 m). Figure 1 illustrates the orbital arrangements for the two pulsars and the magnetotail. The wind from pulsar A blows at pulsar B’s magnetosphere causing B’s magnetospheric material to flow in the radial direction, but because of the orbital motion, the magnetotail is curved behind pulsar B.

The fact that the orbit is almost edge-on to the line of sight makes an eclipse observable each orbit when pulsar A moves behind pulsar B, as shown in Figure 1. The eclipse occurs at orbital longitude of $\sim 90^\circ$ measured from the ascending node and lasts for ~ 30 seconds (Lyne et al. 2004). It was shown that, during an eclipse, the pulsed flux density of A is modulated at the rotational period of pulsar B and its second harmonic (McLaughlin et al. 2004). Synchrotron absorption by the highly relativistic plasma in the closed field-line regions of pulsar B has been proposed as the eclipse mechanism (Lyutikov and Thompson 2005). Modelling of these variations by Breton et al. (2008) gave best-fit values of $\sim 130^\circ$ for the angle between rotation axis and the orbital normal, and $\sim 70^\circ$ for the inclination angle between the rotation and magnetic axes. Hence pulsar A’s radiation passes through pulsar

¹PSR J0737-3039B is currently undetectable at radio frequencies, probably because of relativistic precession of its spin axis (Perera et al. 2010).

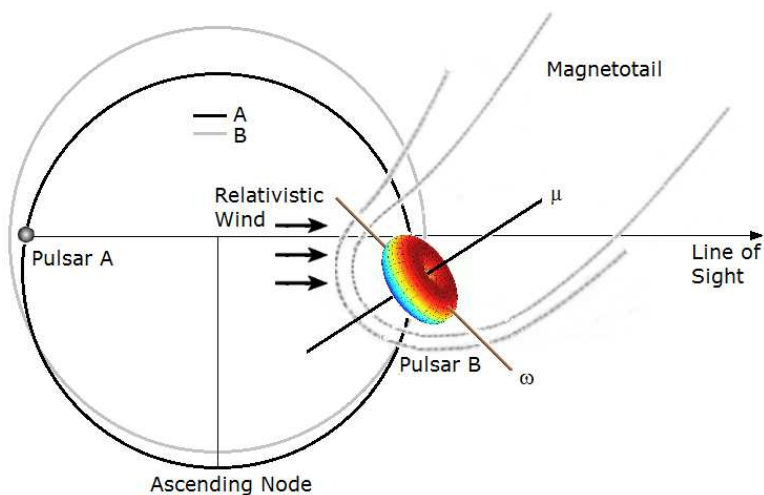


Fig. 1.— Orbital arrangements of the two pulsars and the magnetotail behind pulsar B (not to scale). The black and grey curves represent the orbits for pulsar A and B respectively and both pulsars orbit in the clockwise direction. The shaded areas around pulsar B represent the closed field-line regions (adapted from Breton et al. (2008) and online material), and ω and μ are the angular velocity and magnetic moment vectors respectively. The orbital normal is directed out of the page. As the two pulsars orbit, the radiation we observe from pulsar A first encounters the leading edge of the shock front, enters the magnetosphere of pulsar B, leaves the magnetosphere on the other side and finally crosses the magnetotail.

B’s truncated magnetosphere and interacts with the plasma during an eclipse, then, as the two pulsars advance in orbit away from the superior conjunction, pulsar A’s radiation begins to traverse the magnetotail.

The radiation from pulsar A that penetrates the magnetosphere of pulsar B during and shortly after an eclipse serves as a probe into the plasma content of B’s magnetosphere and magnetotail. Study of the emergent radiation may reveal the largely unknown properties of pulsar magnetospheres and possible physical processes within them. In this paper, we investigate the changes in polarization position angle in radiation from pulsar A at 20 cm and 50 cm wavelengths during and around the eclipses.

2. Observation and data analysis

Our observations of the Double Pulsar use the Parkes 64-m radio telescope. The data of interest were taken in two frequency bands centred at 1369 MHz (20 cm) from September 2007 to October 2011, and at 730 MHz (50 cm) from February 2010 to November 2011. The 20 cm observations were made using the center beam of the 20 cm Multibeam receiver (Staveley-Smith et al. 1996) and the 50 cm observations used the 10 cm/50 cm dual-band receiver (Granet et al. 2005). The Parkes digital filterbank systems, PDFB3 and PDFB4, were used to split the 20 cm and 50 cm data into 1024 and 512 channels respectively, form the polarization products and fold the data at the topocentric pulse period. All observations had a sub-integration time of 30 s. We checked the presence of an eclipse in a data file by checking the coverage of orbital phase of 90° . Once we had identified all relevant data files, regions 10 min before and after the eclipse were retained for further analysis using the PSRCHIVE software suite (Hotan et al. 2004). Spectral band edges were deleted and interference was removed from all files. Files that had significant interference at or close to the eclipse region were eliminated from our list. Short observations of a linearly polarized broad-band calibration signal preceding each pulsar observation were used to calibrate the instrumental phase and gain. For the 20 cm system, the effects of cross-coupling between the orthogonal feed probes were removed as part of the calibration process. Data were summed in frequency using the corrected rotation measure, $+112.3 \text{ rad m}^{-2}$ (Manchester et al. 2010). We obtained 38 files at 20 cm and 13 at 50 cm with good quality data.

To improve the signal-to-noise ratio, we summed the files in each band, binning the results in orbital phase. The phase bins were $\sim 0.7^\circ$ or $\sim 18 \text{ s}$ in width. Sub-integration data were assigned to the two adjacent orbital phase bins with weights proportional to $1 - x$ and x for the leading and trailing bins respectively, where x is the interval between the leading phase bin centre and the sub-integration center time, normalized by the phase bin

width. Finally, Stokes parameters were summed across the main pulse and interpulse to form the average Stokes parameters for each orbital phase bin. This summing of data across the two pulses is possible because the strongly linearly-polarized parts of both pulse components have essentially constant and equal position angle (Demorest et al. 2004).

3. The results

Measurements of the mean position angles and Stokes I (total intensity) for 20 cm and 50 cm wavelengths as a function of orbital phase are presented in Figure 2. Uncertainties in the position angle for each orbital phase were computed using $\sigma = 28.65^\circ(\sigma_I/L_c)$ (Lorimer and Kramer 2005), where σ_I is the standard deviation of the total intensity, and L_c is the linear polarization corrected for noise bias. The Stokes I curves, which are scaled to fit into the plot, clearly show a large drop in intensity representing the eclipse region.

We consistently detected changes in position angle during and shortly after an eclipse at both wavelengths. Inspection of the 20 cm curve in the eclipse region shows that the position angle decreases during the ingress phase with a change of approximately $6^\circ \pm 3^\circ$ relative to the mean baseline level. It then rises to its maximum value of approximately $3^\circ \pm 2^\circ$ above the baseline at the end of the eclipse. It remains high for the following phase bin, then drops back to the baseline value. There are also changes in polarization angle in the corresponding regions during the eclipse at 50 cm, but the uncertainties are larger. Nevertheless, the position angle changes shortly after the eclipse is consistent with those at 20 cm.

We confirmed our results by randomly partitioning the 20 cm files into two subsets as shown in Figure 3. The changes in position angle during the eclipse are essentially consistent between the two subsets, i.e., a decrease during ingress followed by an increase during egress. Partitioning the dataset into either two, three or four subsets, either randomly or chronologically, produced similar results.

4. Mechanisms to change the polarization position angle

4.1. *Synchrotron absorption*

Synchrotron absorption, like synchrotron emission, may be separated into two linearly polarized components, with the more strongly emitted and absorbed component having its electric vector perpendicular to the magnetic field. The polarization-averaged synchrotron

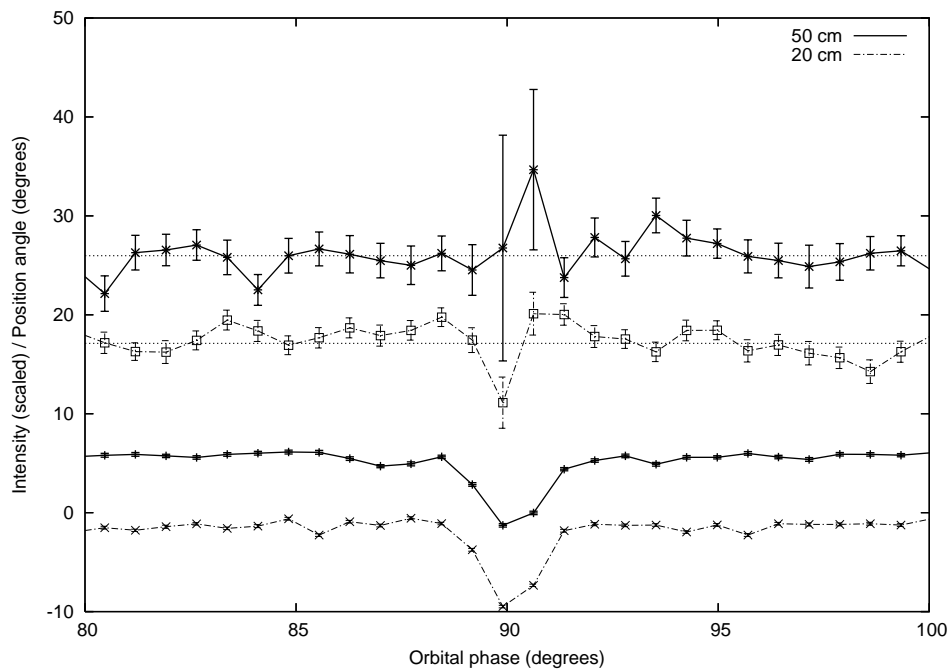


Fig. 2.— Plot of polarization position angle in degrees (upper curves) and Stokes I (total intensity) parameter (lower curves) plotted against orbital phase in degrees for 50 cm (solid curve) and 20 cm (dashed curve) at ~ 18 s time resolution. The curve for position angle at 50 cm is offset by 3° for clarity. The Stokes I curves clearly show the eclipse centred near 90° . The horizontal lines represent average baseline values.

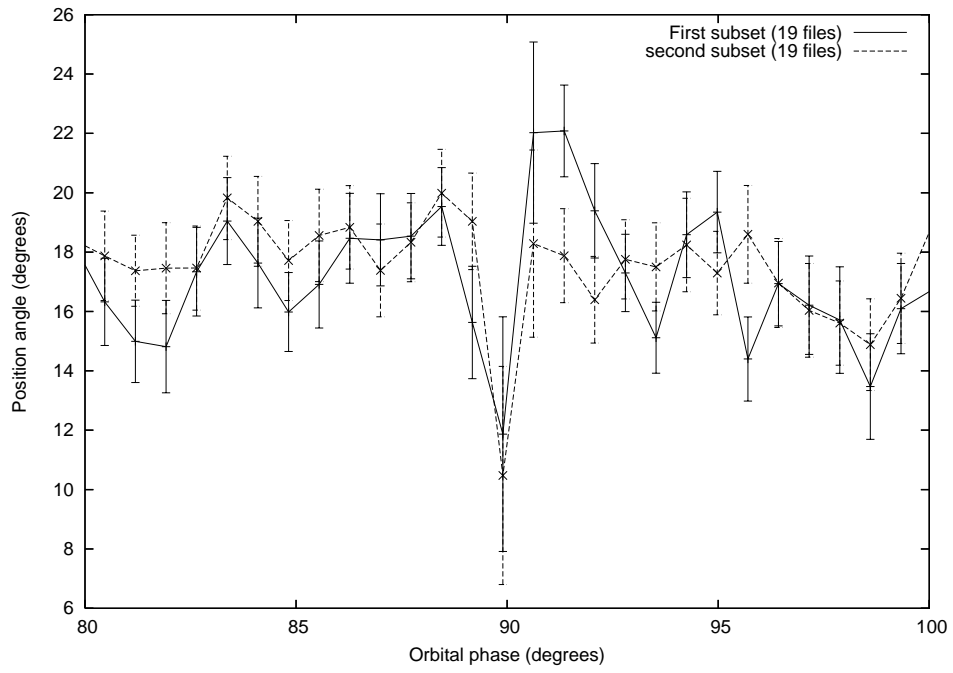


Fig. 3.— Position angles at 20 cm for two subsets of the total data set plotted against orbital phase.

absorption coefficient for a relativistic thermal distribution of particles, $n(\varepsilon) \propto e^{-\varepsilon/k_B T}$, is (Lyutikov and Thompson 2005),

$$\alpha_\nu = \frac{4\pi^2 e n_s}{3^{7/3} B \sin \kappa} \left[\left(\frac{m_e c^2}{k_B T} \right) \frac{\nu_{B,e} \sin \kappa}{\nu} \right]^{5/3}, \quad (1)$$

for $\nu \ll \nu_p \sim 4(k_B T_e/m_e c^2)^2 \nu_{B,e}$, where n_s , B , m_e , c , k_B , T , and ν are the density of the absorbing particles, magnetic field strength, electron mass, speed of light, Boltzmann constant, plasma temperature and radiation frequency respectively, κ is the angle between the magnetic field and propagation vector of the radiation and $\nu_{B,e} = eB/2\pi m_e c$ is the cyclotron frequency. The absorption coefficients for polarization perpendicular and parallel to the magnetic field are $\alpha_\nu^\perp = 4\alpha_\nu/3$ and $\alpha_\nu^\parallel = 2\alpha_\nu/3$, and so $\alpha_\nu^\perp/\alpha_\nu^\parallel = 2$. The optical depth is $\tau_\nu = \alpha_\nu L$, where L is the effective path length through the absorbing medium. Hence, synchrotron absorption preferentially removes the linear polarization perpendicular to the magnetic field. As a result, the position angle of the transmitted radiation changes with increasing optical depth, with the position angle approaching the angle of the projected magnetic field. If χ_0 and χ_ν are the incident and emergent polarization angles relative to the projected magnetic field direction, then,

$$\begin{aligned} I_\nu^\perp &= I_\nu \sin \chi_\nu = I_{0,\nu}^\perp \exp(-\tau_\nu^\perp) = I_{0,\nu} \sin \chi_0 \exp(-4\tau_\nu/3) \\ I_\nu^\parallel &= I_\nu \cos \chi_\nu = I_{0,\nu}^\parallel \exp(-\tau_\nu^\parallel) = I_{0,\nu} \cos \chi_0 \exp(-2\tau_\nu/3). \end{aligned} \quad (2)$$

where $I^{\perp,\parallel}$ represents intensity perpendicular and parallel to the projected magnetic field respectively, and quantities with subscript zero represent incident values at a particular frequency, ν . The change in position angle is given by $\Delta\psi_\nu = (\chi_\nu - \chi_0)$.

4.2. Faraday rotation

The decomposition of linearly polarized radiation into two circular modes that propagate at slightly different phase velocities results in Faraday rotation of the plane of the received linear polarization. Integrating over the full path gives the change in position angle, $\Delta\psi$

$$\Delta\psi \approx 0.81 \lambda^2 \int_0^L n_e B \cos \theta ds = 0.81 L \langle n_e B \rangle \lambda^2 = \text{RM} \lambda^2, \quad (3)$$

where n_e , B and L are the electron density in cm^{-3} , the average magnetic field in microgauss, and the pathlength in parsecs respectively, and $\cos \theta$ is the angle between the magnetic field and the ray path, RM is the rotation measure. The notation $\langle \dots \rangle$ implies an average along the ray path.

Pulsar magnetospheres are thought to be populated with highly relativistic plasma. If there is no thermal plasma present, as some models imply, the modes would be nearly linearly polarized, and conventional Faraday rotation would not occur. The natural wave modes would also be linear if the density of the electrons and positrons were the same. The circular component needed can arise from the net charge, associated with the Goldreich-Julian density, provided the particle energies are not highly relativistic. Any measured Faraday rotation would have the interesting implication that the dominant contribution to the wave dispersion is from electrons that are no more than mildly relativistic.

5. Discussion

5.1. *Changes in position angle during the eclipse*

Our measurements of the position angle change of A’s pulse emission integrate over the rotation of B’s magnetosphere and the resulting eclipse modulation, with our 18 s averaging time covering approximately 6.5 revolutions of B. The direction of the differential synchrotron absorption relative to the incoming radiation will vary during B’s rotation and along the path through the magnetosphere. It will also change as the line of sight to A moves through B’s magnetosphere because of the orbital motion. Our present results do not justify a full computation of this complex variation. However, we can approximate the effect by recognising that the closed field lines perpendicular to the magnetic axis are symmetrical but of opposite sign in the two hemispheres. As the star rotates, they will therefore average to zero leaving a net magnetic field along the magnetic axis. Furthermore, since the magnetic and rotation axes are not aligned, the field perpendicular to the rotation axis will also cancel leaving a net magnetic field along the rotation axis of B. During the four years covered by our observations, B’s spin axis will precess by about 20° but this will have little effect of the observed absorption which is dominated by averaging over B’s rotation

The peaks and dips in flux density from pulsar A in the eclipse light curve (McLaughlin et al. 2004) imply that the optical depth is, respectively, either ~ 0 when the line of sight misses B’s magnetospheric torus, or > 1 , which corresponds to the absorbing closed-field region that obstructs our view of pulsar A resulting in a large decline in flux density. The differential changes in I_ν^\perp and I_ν^\parallel would be insignificant during most of the eclipse region where $\tau > 1$ because the intensities are low, except near the boundaries of the eclipse where the optical depth $\tau \sim 1$, which characterizes the applicability of Equation (2). For the synchrotron absorption model (Equation 1), the density of the absorbing plasma can be estimated by $n_s = M n_{GJ}$, where $M = 10^6$ is the pair multiplicity parameter, and n_{GJ} is the Goldreich and Julian (1969) charge density. The energy balance between A’s relativistic

wind and B’s magnetic pressure gives a field strength of 7 G at the eclipse boundary, which is estimated to be near $r_{\text{bal}} \approx r_L/10 \sim 1.5 \times 10^9$ cm from pulsar B (Lyutikov and Thompson 2005), and so $n_{GJ} \sim 0.2 \text{ cm}^{-3}$, giving $n_s \sim 2 \times 10^5 \text{ cm}^{-3}$. The cyclotron frequency, $\nu_{B,e}$ is 2×10^7 Hz, and the relativistic electrons are assumed to be thermally distributed at temperature $(k_B T/m_e c^2) = 10$. Assuming B’s magnetic field is randomly oriented and averaging between 0° and 90° gives $\langle (\sin \kappa)^{2/3} \rangle \approx 2/\pi$, and with $L = r_{\text{bal}}$, we obtain $\langle \tau_{20} \rangle \sim 1$ and $\langle \tau_{50} \rangle \sim 3$, where the number in subscript represents the wavelength. Using these values and our data for the total intensity, and assuming $\chi_0 = 45^\circ$, Equation (2) gives an order of magnitude change in polarization or position angle of 10° , consistent with our measurements. We therefore, conclude that differential synchrotron absorption in the closed field-line regions can plausibly account for the observed position angle changes during the eclipse.

Combining Equation (2) and rearranging gives $\tan \chi_\nu = \tan(\chi_0 + \Delta\psi_\nu) = \tan \chi_0 \exp(-2\tau_\nu/3)$. In principle, with higher time-resolution observations of the eclipse, one could use this equation to determine the angle of the rotation axis of pulsar B projected on the sky, $\psi_{B,\Omega}$. At times when τ_ν is neither very large nor very small, both τ_ν and $\Delta\psi_\nu$ may be measurable. Since $\chi_0 = \psi_0 - \psi_{B,\Omega}$ and $\Delta\psi_\nu = \chi_\nu - \chi_0 = \psi_\nu - \psi_0$, the above equation can be rewritten as $\tan(\psi_\nu - \psi_{B,\Omega}) = \tan(\psi_0 - \psi_{B,\Omega}) \exp(-2\tau_\nu/3)$. With multiple measurements for each of ψ_ν and τ_ν , and since ψ_0 is known, $\psi_{B,\Omega}$ may be determined.

5.2. Changes in position angle due to Faraday rotation

After the eclipse, the synchrotron absorption effect will diminish and Faraday rotation should start to manifest. During this time, pulsar A’s radiation goes through regions located immediately beyond the closed field-line boundaries in the wind zone where the oppositely directed magnetic fields in the two lobes from the magnetotail each connect to one of the polar caps. Unlike the geomagnetotail where field structure is symmetric in these regions (Pilipp and Morfill 1978), the large inclination angle results in an asymmetric field structure between the two lobes in these regions and an alternating field structure as the pulsar rotates within the confining magnetosheath (Spitkovsky and Arons 2004). With the misalignment between the rotation axis and the orbital normal, a net magnetic field in the line of sight will result in Faraday rotation in radiation that traverses these regions of pulsar B’s magnetotail.

Faraday rotation causes changes in position angle of the same sign at both wavelengths shortly after an eclipse. The measured changes in position angle can be used to estimate $\langle n_e B \rangle L$, and a separate estimate of L and B allows n_e to be estimated in the magnetotail. Consider mean values along the line of sight, and assuming magnetic field scales as $\propto r^{-2}$ up

to $L/2$ in the magnetotail² gives $B \sim 2$ G, where $L \approx 1.5 \times 10^{-8}$ pc is the semi-major axis of pulsar B's orbit. Equation (3), with $\Delta\psi_{50} \sim -5^\circ$, gives $n_e \sim 40 \text{ cm}^{-3}$. The corotating charge density (Goldreich and Julian 1969) is the difference between the number densities of positrons and electrons, which gives $\sim 20 \text{ cm}^{-3}$ at $r = r_{\text{bal}}$. Although the corotation requirement does not apply beyond r_{bal} , the wind in the magnetotail rotates with the star implying a charge density of order the Goldreich-Julian value. This suggests that Faraday rotation may be responsible for the changes in position angle away from the eclipse region. As mentioned earlier, the complication in interpreting the results lies in the complex variations in the orientation of B's magnetic field structure, caused by field reversals between the two lobes in the magnetotail, the large inclination angle between magnetic and rotation axes of pulsar B and the orbital motion of the two pulsars. However, with higher time resolution, it is possible that changes in A's position angle could be correlated with different orientations of B's field structure.

5.3. Mildly relativistic particle energies

Faraday rotation in the magnetotail would require that the charged particles be no more than mildly relativistic. If the particles were highly relativistic, the natural wave modes would be linearly polarized and there would be no Faraday rotation. If our suggestion that significant Faraday rotation occurs is confirmed by more detailed observations, it would be a strong indication that the bulk of the pairs produced in a pulsar magnetosphere are no more than mildly relativistic. This is inconsistent with theories for the pair creation that suggest much higher mean Lorentz factors of typically $\gamma \sim 10^2 - 10^4$ (Sturrock 1971; Ruderman and Sutherland 1975; Daugherty and Harding 1982). Since energy-loss mechanisms are ineffective (Ruderman and Sutherland 1975; Sturmer 1995; Lyubarskii and Petrova 2000), any nonrelativistic plasma must be created directly in the pulsar magnetosphere (Jessner et al. 2001). Direct generation of mildly relativistic pairs is favored for magnetic fields with $0.02 B_{\text{cr}} < B < 0.1 B_{\text{cr}}$, where $B_{\text{cr}} \approx 4.9 \times 10^{13}$ G is the critical field strength (Weise and Melrose 2002).

²Scaling of the magnetic field strength in the open field-line region and magnetotail is uncertain but not critical to our discussion.

6. Conclusions

We have confirmed the changes in polarization position angle in radiation from pulsar A during and shortly after the eclipse in the Double Pulsar system at 20 cm and 50 cm wavelengths. The changes are $\sim 2\sigma$ at 20 cm and $\sim 1\sigma$ at 50 cm. The variations at 20 cm were confirmed by partitioning the data files into two subsets. Differential synchrotron absorption in the closed field-line regions can account for the observed position angle changes during the eclipse. Modelling of the changes in position angle shortly after the eclipse with Faraday rotation gives a charge density that is consistent with the Goldreich-Julian value. Since energy-loss mechanisms in pulsar magnetospheres are inefficient, the presence of Faraday rotation implies that pairs must be created directly in nonrelativistic regime.

Acknowledgments

We thank our colleagues for assistance with the observations reported in this paper. The Parkes radio telescope is part of the Australia Telescope National Facility which is funded by the Commonwealth of Australia for operation as a National Facility managed by CSIRO. Pulsar research at UBC is supported by an NSERC Discovery Grant.

REFERENCES

- Arons, J., Backer, D. C., Spitkovsky, A., and Kaspi, V. M.: 2004, *Proc. 2004 Apsen Winter Conf. on Astrophysics, Binary Radio Pulsars*, San Francisco: ASP
- Breton, R. P., Kaspi, V. M., Kramer, M., McLaughlin, M. A., and et al.: 2008, *Science* **321**, 104
- Burgay, M., D’Amico, N., Possenti, A., Manchester, R. N., and et al.: 2003, *Nature* **426**, 531
- Daugherty, J. K. and Harding, A. K.: 1982, *ApJ* **252**, 337
- Demorest, P., Ramachandran, R., Backer, D. C., Ransom, S. M., Kaspi, V., Arons, J., and Spitkovsky, A.: 2004, *ApJ* **615**, L137
- Goldreich, P. and Julian, W. H.: 1969, *ApJ* **157**, 869

- Granet, C., Zhang, H. Z., Forsyth, A. R., Graves, G. R., Doherty, P., Greene, K. J., James, G. L., Sykes, P., Bird, T. S., Sinclair, M. W., Moorey, G., and Manchester, R. N.: 2005, *ieeetap* **47**, 13
- Hotan, A. W., van Straten, W., and Manchester, R. N.: 2004, *Publications of the Astronomical Society of Australia* **21**, 302
- Jessner, A., Lesch, H., and Kunzl, T.: 2001, *ApJ* **547**, 959
- Kramer, M., Stairs, I. H., Manchester, R. N., McLaughlin, M. A., and Lyne, A. G.: 2006, *Science* **314**, 97
- Lorimer, D. R. and Kramer, M.: 2005, *Handbook of Pulsar Astronomy*, Cambridge
- Lyne, A. G., Burgay, M., Kramer, M., Possenti, A., Manchester, R. N., and et al.: 2004, *Science* **303**, 1153
- Lyubarskii, Y. E. and Petrova, S. A.: 2000, *Astron. Astrophys.* **355**, 406
- Lyutikov, M. and Thompson, C.: 2005, *ApJ* **634**, 1223
- Manchester, R. N., Kramer, M., Stairs, I. H., Burgay, M., Camilo, F., Hobbs, G. B., Lorimer, D. R., Lyne, A. G., McLaughlin, M. A., McPhee, C. A., Possenti, A., Reynolds, J. E., and van Straten, W.: 2010, *ApJ* **710**, 1694
- McLaughlin, M. A., Lyne, A. G., Lorimer, D. R., Possenti, A., Manchester, R. N., and et al.: 2004, *ApJ* 616(L131)
- Perera, B. B. P., McLaughlin, M. A., Kramer, M., Stairs, I. H., and et al.: 2010, *ApJ* **721**, 1193
- Pilipp, W. G. and Morfill, G.: 1978, *Journal of Geophysical Research* **83**, 5670
- Ruderman, M. and Sutherland, P. G.: 1975, *ApJ* **196**, 51
- Spitkovsky, A. and Arons, J.: 2004, *Bulletin of the American Astronomical Society, HEAD meeting* **36(8, 08.02)**, 917
- Staveley-Smith, L., Wilson, W. E., Bird, T. S., Disney, M. J., Ekers, R. D., Freeman, K. C., Haynes, R. F., Sinclair, M. W., Vaile, R. A., Webster, R. L., and Wright, A. E.: 1996, *PASA* **13**, 243
- Sturmer, S. J.: 1995, *ApJ* **446**, 292

Sturrock, P.: 1971, *ApJ* **164**, 529

Weise, J. I. and Melrose, D. B.: 2002, *MNRAS* **329**, 115